Supplementary Information

Subwavelength direct-write nanopatterning using optically trapped microspheres:

Euan McLeod and Craig B. Arnold

Mechanical & Aerospace Engineering Department, Engineering Quadrangle, Princeton University, Princeton, NJ 08544

Supplemental Discussion: Positional Uncertainties

The fundamental limit governing the positional accuracy of the technique is the Brownian motion of the microsphere within the optical trap. In our cylindrical geometry, the probability of finding a particle in a region between *r* and *r* + *dr* is given by,

$$P(r)dr = 2\pi r A \exp\left(-\frac{U(r)}{kT}\right)dr, \qquad (1)$$

where *A* is a normalization constant, *U(r)* is the potential energy of the radiation field, *k* is Boltzmann's constant, and *T* is the temperature. Although our 0.76 μm particles are larger than the optical trapping wavelength, we will still approximate the optical potential using the Rayleigh scattering model because it provides insight into the physics of the trap stability without requiring Mie theory calculations. The potential energy due to the gradient force on a Rayleigh particle is given in MKS units by[1],

$$U(r) = -\frac{2\pi n_b a^3}{c}\left(\frac{\left(n_p / n_b\right)^2 - 1}{\left(n_p / n_b\right)^2 + 2}\right) I(r), \qquad (2)$$

where n_b is the refractive index of the surrounding medium, n_p is the refractive index of the particle, *a* is the radius of the particle, *c* is the speed of light, and *I(r)* is the intensity of the trapping laser beam, in our case given by the profile shown in Fig. S1:

$$I(r) = \frac{P_0}{0.85a^2} J_0{}^2\left(\frac{2.40r}{a}\right), \qquad (3)$$

assuming the Bessel beam is appropriately scaled so that the radius of the central lobe is equal to the radius of the trapped particle, P_0 is the power in the central lobe of the Bessel beam, *a* is the particle radius, and 2.40 is first zero of $J_0{}^2(x)$.

Using a polystyrene particle of radius *a* = 380 nm and a Bessel beam with 100 μW of power in the central lobe, we calculate the mean positional error to be $\langle r \rangle$ = 32 nm at room temperature. This positional error can be reduced by increasing the trapping laser

power, however there is an upper limit which depends on the electrostatic sphere-surface repulsive force as discussed below.

As a first approximation, we can treat the thermal field in the liquid as being constant in time. The continuous trapping laser will lead to an increased, but constant, temperature. This constant thermal field in the liquid has a minimal effect on the positional uncertainty. If instead of being at room temperature, the system were just below the boiling point of water at 373 K, then the positional uncertainty would increase to 36 nm. The processing laser will also have an effect on the thermal field within the liquid, however this effect should occur at timescales much shorter than our procedure, because we are using a nanosecond laser, but firing shots at rates less than 100 Hz. Hence, this should not affect positional error.

Ablative material removal may temporarily displace the bead from the centre of the trap until the optical force restores the particle to the centre position. We observed this in the upper range of fluences used for nanopatterning, when features such as those in Fig. 4c were formed. In such situations writing rates need to be reduced somewhat to allow the bead to return to the centre of the trap before the subsequent shot. We wrote features at rates ranging from 1 to 100 Hz, depending on the distance between shots, laser trapping power, and pulsed laser fluence.

Sample translation can also lead to positional error. If writing speeds are increased too much, the particle may be lost from the trap when the Stokes drag exceeds the trapping laser force on the particle. An external fluid flow would have the same effect. We found that writing speeds on the order of microns per second still provided consistent positioning accuracy.

Sharp, pre-existing asperities can also lead to positional error because the resulting surface repulsion force is not normal to the trapping beam. However, a higher power trapping laser can help to mitigate these uncertainties.

There are some factors which *do not* affect positional error that should be noted. First the optical scattering force induced on the bead from the pulsed laser is negligible compared to the continuous trapping laser force. At our fluences, the impulse from the pulsed laser is on the order of FA/c, where F is the fluence, A is the cross-sectional area of the particle, and c is the speed of light[2]. This results in an impulse on the order of 10^{-18} N s. Assuming a Stokes drag force of $-6\pi\eta a v$, where η is the dynamic viscosity of water and v is the particle velocity results in a maximum displacement on the order of Angstroms.

Second, due to the low Reynolds number of the system, the motion of a microscopic particle in water is always overdamped, and therefore there is no significant harmonic motion of the particle within an optical trapping potential

In future experiments, we will experimentally characterize the above effects on the positional accuracy of our technique.

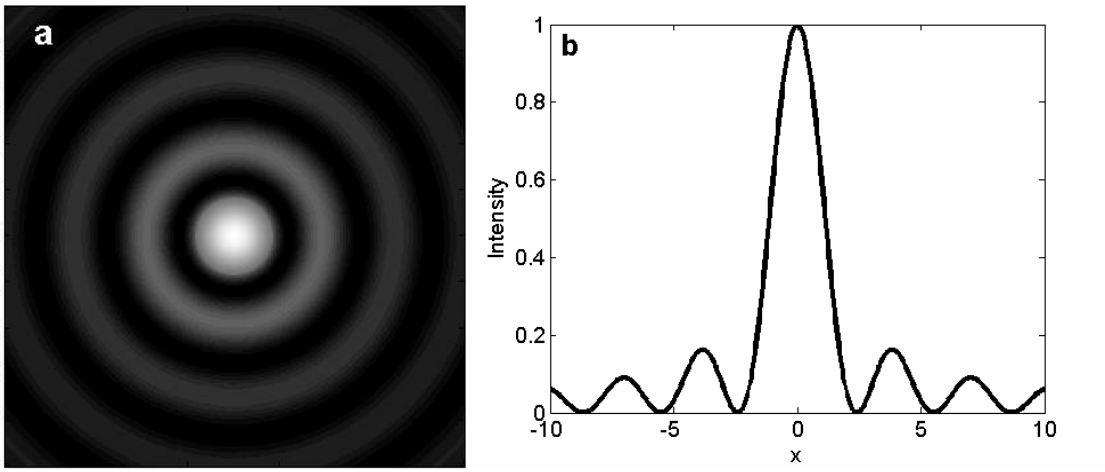

Fig. S1. Bessel beam profiles. **(A)** Plan view showing the calculated transverse intensity variations of a Bessel beam. **(B)** Cross section of **A** illustrating the high intensity of the central peak.

Supplementary Discussion: Sphere-Surface Spacing

The sphere-surface spacing is determined by the balance between the laser forward radiation pressure force and a repulsive electrostatic double-layer force resulting in the self-positioning depicted in Fig. S3.

As was done in the above Positional Uncertainties section, the probability of the spacing between the particle and substrate being between z and $z + dz$ is given by,

$$P(z)dz = B\exp\left(-\frac{U_l(z)+U_{dl}(z)}{kT}\right)dz, \qquad (4)$$

where B is a normalization constant, and $U_l(z)$ is the potential induced by the laser radiation pressure, and $U_{dl}(z)$ is the potential from the double layer. In order to keep the equations simple, we will assume Rayleigh regime optical trapping as above, a Debye length (κ^{-1}) smaller than the microsphere radius, and equal surface potentials for the sphere and substrate (ψ_0). With such assumptions, the potentials will be given by[3, 4],

$$U_l(z) = \frac{128\pi^5 a^6 I_0 n_b}{3c\lambda^4}\left(\frac{(n_p/n_b)^2-1}{(n_p/n_b)^2+2}\right)^2 z \qquad (5)$$

$$U_{dl}(z) = \varepsilon\varepsilon_0 a\psi_0^{\,2}\log\left(1+e^{-\kappa z}\right), \qquad (6)$$

where I_0 is the mean intensity incident on the microsphere, ε is the dielectric constant of water, and ε_0 is the free-space permittivity.

While the specific values of κ, ψ_0, and I_0 were not measured for our systems, we can use some reasonable test values to arrive at approximate sphere-surface spacings[4].

Setting κ^{-1} = 100 nm and ψ_0 = 90 mV and choosing the optical power passing through the bead to be P_0 = 100 μW, the resulting mean surface spacing is $\langle z \rangle = 50$ nm, and the positional error is given by $\left(\langle z^2 \rangle - \langle z \rangle^2 \right)^{1/2}$ = 9 nm. The mean surface spacing can also be determined by balancing the laser radiation pressure force with the electrostatic double layer repulsion (Fig S2). If the temperature were raised to 373 K, then the mean spacing would not change, and the spacing error would increase to 10 nm.

Several effects can alter the equilibrium sphere-surface spacing. Adding more electrolyte to the trapping solution can decrease the Debye length, resulting in a closer spacing. Modifying the surface chemistry of the sphere and substrate will alter the surface potentials. Higher surface potentials increase sphere-surface spacing. Increasing the laser power will decrease sphere-surface spacing. However, because the electrostatic double-layer repulsion reaches a finite maximum at $z = 0$, there is an upper limit on the trapping laser power so as to avoid contact and the resulting Van der Waals adhesion between the sphere and the substrate (see Fig. S2).

The factors in the above Positional Uncertainties section that lead to transverse positional uncertainties can also lead to longitudinal positional uncertainties.

For most of our theoretical calculations, we have assumed a separation distance of 50 nm based on the above reasoning. Using this separation distance, we find good agreement between theoretical spot sizes and experimental predictions for small beads in Fig. 2. However, as predicted above, the spacing should have some dependence on sphere size, and this explains the discrepancies in Fig. 2 between the theory and experiment for larger bead sizes.

In future experiments, we will incorporate an *in situ* apparatus for measuring sphere-surface height, either based on total internal reflection microscopy[5] or by comparing the diffraction rings of a trapped bead and a bead adhered to the substrate[6].

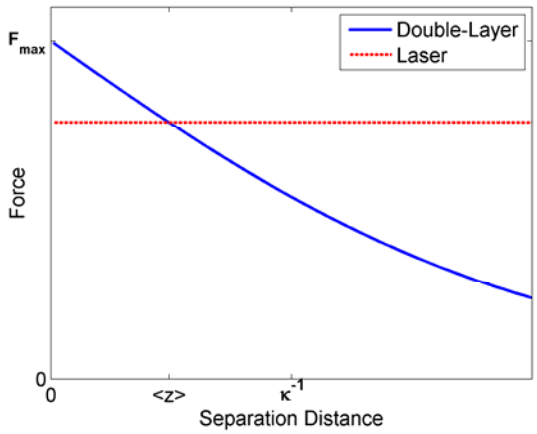

Fig. S2. Force balance between the laser and the electrostatic double layer. The forces are calculated by taking the derivatives with respect to z of Eqs. 5 and 6. The equilibrium sphere-surface separation will occur at $\langle z \rangle$, where the absolute forces of the

double-layer and laser pressure are equal. According to the above theory, κ^{-1} is the Debye length and $F_{\max} = \frac{1}{2}\varepsilon\varepsilon_0 a \psi_0^{\,2}\kappa$.

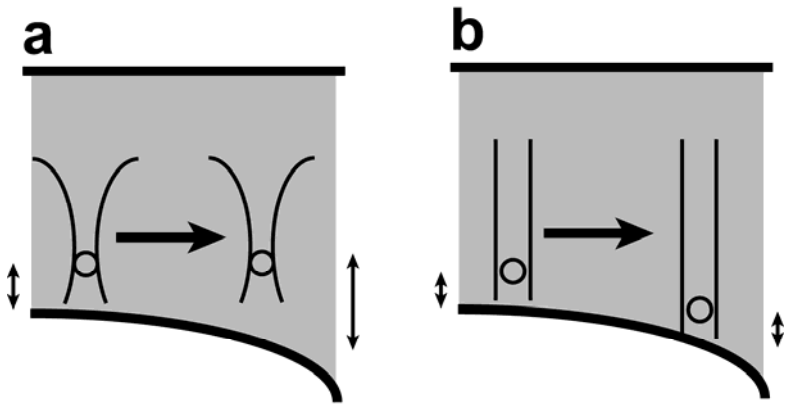

Fig. S3. Self-positioning of particles using Bessel traps. **(A)** Standard Gaussian traps produce gradients in all three directions leading to a fixed position for the trapped particle. Therefore they do not maintain sphere-surface spacing as the substrate changes height, either due to roughness or existing surface features. (**B)** Bessel traps exhibit gradients in the transverse direction. A scattering force in the propagation direction causes the particle to be pushed towards the surface. Force balance due to repulsive forces from the fluid and substrate maintain sphere-surface spacing regardless of the absolute height of the substrate and enable the self-positioning effect.

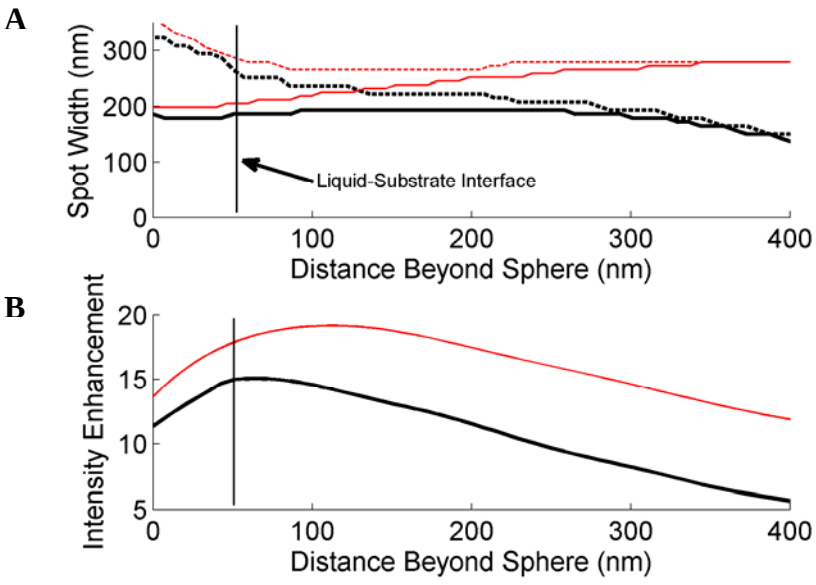

Fig. S4. FDTD Simulations for a 0.76 μm sphere illustrating the effect of the substrate on the pulsed laser fluence distribution. The sphere-substrate separation distance is 50 nm. **(A)** The width, in both the polarisation (dashed) and other transverse direction (solid), of the region where the fluence surpasses the material threshold (48 mJ cm^{-2}) for

a 12 mJ cm^{-2} incident pulse. Thick black lines correspond to the model for an absorbing polyimide substrate. Thin red lines correspond to the model without a substrate. Note that at the substrate surface, the difference in spot size is less than 10% between the models with and without the substrate. This small change indicates the lack of a resonance between the sphere and substrate due to the highly absorbing nature of the dielectric substrate. This is investigated further in Fig. S5. **(B)** The intensity enhancement predicted as a function of the distance beyond the substrate. Colours are the same as in (A).

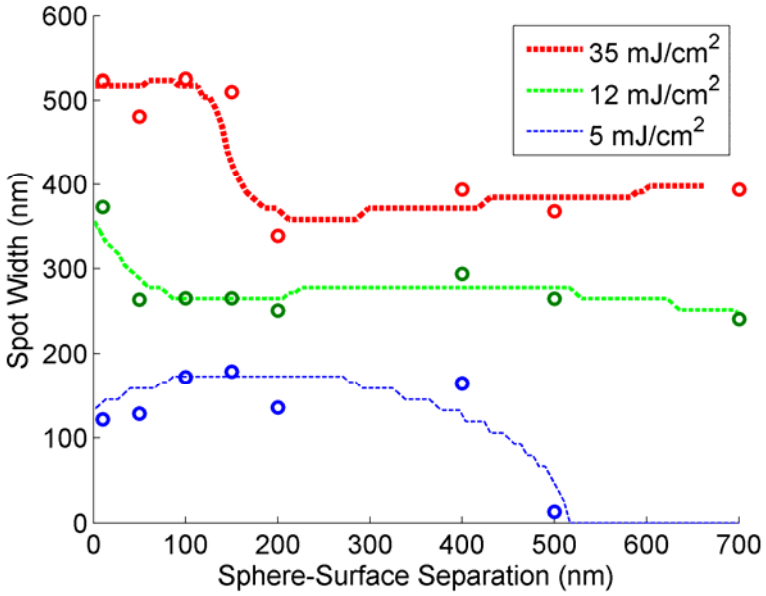

Fig. S5. FDTD Simulations for a 0.76 μm sphere illustrating the effect of the sphere-substrate separation on the spot size at the surface. Hollow circles represent simulations for the system that have explicitly included a polyimide substrate. Dashed lines indicate estimates based on a model of a sphere surrounded entirely by water without a substrate. Colour indicates the incident laser fluence on the sphere. As can be seen by the good agreement between lines and circles, the substrate has a minimal effect on the spatial size of the sphere-focused pulse at the surface because the polyimide substrate is an absorbing dielectric. Spot sizes are calculated in the polarisation direction the same way as in Fig. S4: the width of the region where the fluence surpasses the material threshold (48 mJ cm^{-2}). Note that for small spot sizes, maintaining accurate sphere-surface spacing is necessary to achieve consistent spot sizes.

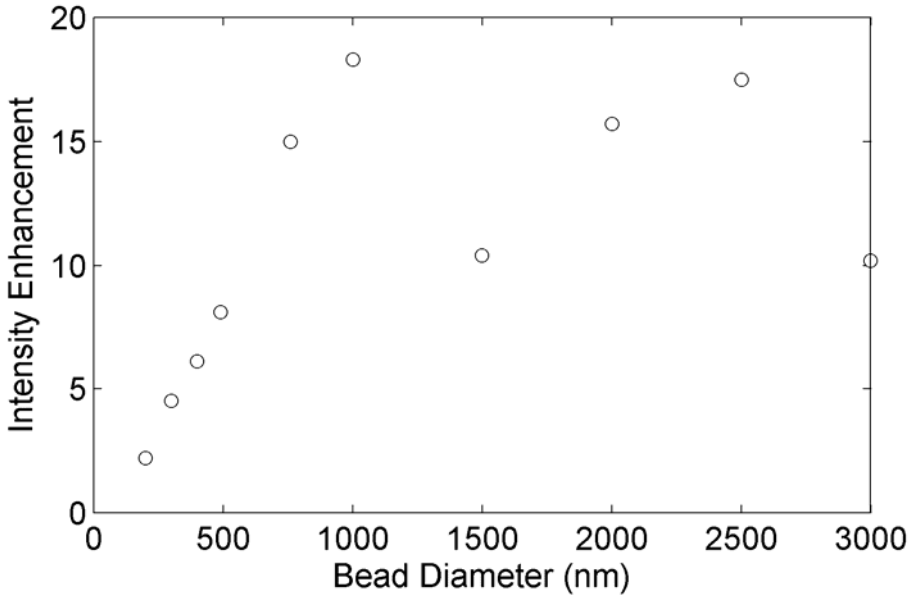

Fig. S6. Simulated Intensity Enhancements. Calculations were performed with a polyimide substrate 50 nm away from polystyrene microspheres. Note that intensity enhancements fall rapidly for sphere sizes less than 0.76 μm, however they do not dramatically increase for larger spheres. Higher enhancements for larger spheres would be realized if the sphere-surface spacing were increased.

REFERENCES:

1. Harada, Y. & Asakura, T. Radiation forces on a dielectric sphere in the Rayleigh scattering regime. *Opt. Commun.* 124, 529-541 (1996).
2. Ashkin, A. Acceleration and Trapping of Particles by Radiation Pressure. *Physical Review Letters* 24, 156-159 (1970).
3. Ashkin, A., Dziedzik, J. M., Bjorkholm, J. E. & Chu, S. Observation of a Single-Beam Gradient Force Optical Trap for Dielectric Particles. *Optics Letters* 11, 288-290 (1986).
4. Verwey, E. J. W. & Overbeek, J. T. G. *Theory of the Stability of Lyophobic Colloids* (Elsevier Publishing Company, Inc., 1948).
5. Behrens, S. H., Plewa, J. & Grier, D. G. Measuring a colloidal particle's interaction with a flat surface under nonequilibrium conditions. *Eur. Phys. J. E* 10, 115-121 (2003).
6. Hansen, P. M., Dreyer, J. K., Ferkinghoff-Borg, J. & Oddershede, L. Novel optical and statistical methods reveal colloid-wall interactions inconsistent with DLVO and Lifshitz theories. *J. Colloid Interf. Sci.* 287, 561-571 (2005).